Transient Full Maxwell Computation of Slow Processes

J. Ostrowski, R. Hiptmair, F. Krämer, J. Smajic, and T. Steinmetz

Abstract This article deals with finite element solution of the full linear Maxwell's equations. The focus lies on the transient simulation of slow processes, i.e. of processes, where wave propagation does not play a role. We employ an implicit Euler method for time discretization of the $\mathbf{A}, \varphi$-based Galerkin-formulation with Coulomb-gauge. We propose a novel stabilization technique that makes possible the use of very large timesteps. This is of supreme importance for efficient simulation of slow processes in order to keep the number of timesteps reasonably small. The greatly improved robustness in comparison with a standard formulation is demonstrated through numerical experiments. As an example we simulate the *lightning impulse test* of an industrial dry-type transformer.

1 Motivation

Electromagnetic field simulations of slow processes, i.e. of processes in the so-called *low frequency range*, where wave propagation does not play a role, are normally carried out by using either [8]

- A static model, i.e. *electrostatics* or *magnetostatics*, if all variations in time can be neglected.
- Or a quasi-static model, i.e. *electro-quasistatics* or *magneto-quasistatics*.

J. Ostrowski (✉) · J. Smajic · T. Steinmetz
ABB Switzerland Ltd., Corporate Research, Segelhofstr. 1 K, CH-5405 Baden, Switzerland
e-mail: joerg.ostrowski@ch.abb.com; jasmin.smajic@ch.abb.com;
thorsten.steinmetz@ch.abb.com

R. Hiptmair · F. Krämer
Seminar for Applied Mathematics, ETH Zürich, Rämistr. 101, 8092 Zurich, Switzerland
e-mail: hiptmair@sam.math.ethz.ch; floriankra@gmail.com

B. Michielsen and J.-R. Poirier (eds.), *Scientific Computing in Electrical Engineering SCEE 2010*, Mathematics in Industry 16, DOI 10.1007/978-3-642-22453-9_10,

The static models are just special cases of the full Maxwell's equations, whereas the quasi-static models are approximations that are only valid in special situations [10,11]. If capacitive effects are dominant and the magnetic field energy is negligible against the electric field energy, then the electro-quasistatic model can be used, but induction is neglected. On the contrary, if inductive effects matter and the electric field energy is negligible versus the magnetic field energy, then the magneto-quasistatic model (or eddy-current model) can be used. The displacement-current is neglected in the magneto-quasistatic model.

This zoo of models forces the computational engineer to acquire and learn several simulation modules to cover the wide range of industrial applications. Some expertise in electromagnetics is also required in order to select the appropriate model. This is not desirable, because it limits the possible users of electromagnetic field simulation to a circle of experts. Moreover, the quasi-static models do not allow the simulation of configurations with coupled inductive/capacitive effects. For these reasons, we propose a generally applicable full Maxwell solver that unifies the four models of the low frequency range. However, standard full Maxwell formulations lack stability in this range. Therefore we describe a remedy in the form of a particular stabilization. Through this we achieve a robust Maxwell formulation.

We structured our article like this: first we analyze the reason for the instability of the standard full Maxwell formulation. Next we add the stabilization. Since this technique has already been introduced in frequency domain [3], we focus here on its realization in time domain. We demonstrate the strongly improved robustness by numerical experiments. At the end we show an industrial application of a transient simulation.

2 Instability of the Full Maxwell Model

We assume that the bounded computational domain $\Omega = \Omega_c \cup \Omega_n$ consists of a conductive domain Ω_c and a non-conductive domain Ω_n. For completeness we include possible prescribed solenoidal currents $\mathbf{j}^s$ and prescribed charges $\rho^s := -\mathrm{div}\mathbf{j}^{s\rho}$. We assume stationary, i.e. non-moving, and non-deforming ohmic conductors. Thus the current is $\mathbf{j} = \sigma \cdot \mathbf{E} + \mathbf{j}^s$. We use an implicit Euler scheme for time discretization, because we deal with an essentially dissipative regime. With these definitions the standard Coulomb gauged $\mathbf{A}, \varphi$-based full Maxwell formulation that has to be solved in each timestep (k) writes

$$\mathbf{curl}\,\frac{1}{\mu}\,\mathbf{curl}\,\mathbf{A}_k + \left(\frac{\varepsilon}{\triangle t^2} + \frac{\sigma}{\triangle t}\right)\mathbf{A}_k + \left(\frac{\varepsilon}{\triangle t} + \sigma\right)\mathbf{grad}\,\varphi_k \tag{1}$$

$$= \left(\frac{2\varepsilon}{\triangle t^2} + \frac{\sigma}{\triangle t}\right)\mathbf{A}_{k-1} - \frac{\varepsilon}{\triangle t^2}\mathbf{A}_{k-2} + \frac{\varepsilon}{\triangle t}\,\mathbf{grad}\,\varphi_{k-1} + \mathbf{j}_k^s + \frac{\mathbf{j}_k^{s\rho} - \mathbf{j}_{k-1}^{s\rho}}{\triangle t} \text{ in } \Omega,$$

$$\mathrm{div}(\varepsilon\mathbf{A}_k) = 0 \text{ in } \Omega\,. \tag{2}$$

Herein $\triangle t$ is the size of the timestep and μ, ε and σ are material coefficients. The boundary conditions are chosen such that they model the contacts, see [3, 4]. In [3] it was explained that in frequency domain this standard formulation lacks stability in the stationary limit, i.e. for vanishing angular frequency $\omega \to 0$. The same instability occurs in the time-domain for large timesteps $\triangle t$ due to the equivalence of $i\omega$ in the frequency domain with $\frac{1}{\triangle t}$ in the time domain. The reason for the instability is the fact that for $\frac{1}{\triangle t} \to 0$ the electric scalar potential φ is not controlled by (1) and (2) in the non-conducting domain Ω_n (where $\sigma = 0$). As a consequence, φ becomes undetermined locally, and the electric field cannot be recovered in Ω_n. Theoretically, this is only the case at $\frac{1}{\triangle t} = 0$, but in computations one observes severe ill-conditioning already for positive but small $\frac{1}{\triangle t}$. This is caused by the very small parameter ε in the crucial term $\frac{\varepsilon}{\triangle t}\,\mathbf{grad}\,\varphi_k$ of (1).

This instability also haunts other standard formulations. If, for example, *temporal gauge* is used, where the electric scalar potential is set to zero, then we have to solve the system

$$\mathbf{curl}\,\frac{1}{\mu}\,\mathbf{curl}\,\mathbf{A}_k + \left(\frac{\varepsilon}{\triangle t^2} + \frac{\sigma}{\triangle t}\right)\mathbf{A}_k \tag{3}$$

$$= \left(\frac{2\varepsilon}{\triangle t^2} + \frac{\sigma}{\triangle t}\right)\mathbf{A}_{k-1} - \frac{\varepsilon}{\triangle t^2}\mathbf{A}_{k-2} + \mathbf{j}_k^s + \frac{\mathbf{j}_k^{s\rho} - \mathbf{j}_{k-1}^{s\rho}}{\triangle t} \quad \text{in} \quad \Omega\,,$$

$$\varphi = 0 \quad \text{in} \quad \Omega\,. \tag{4}$$

In this formulation we lose uniqueness of $\mathbf{A}_k$ in the non-conducting domain for large timesteps $\triangle t \to \infty$. In the limit, any gradient may be added to the solution of $\mathbf{A}$ in the non-conducting domain. Consequently the electric field is also poorly controlled for large $\triangle t$ in temporal gauge, as is strikingly illustrated in Sect. 4. The same holds for the equivalent $\mathbf{E}$*-based formulation*. If the gauge is removed in the *ungauged formulation* (i.e. only (1)), then one loses control of both φ and $\mathbf{A}$ in Ω_n. Again, the electric field cannot be recovered in Ω_n.

3 Stabilization

Stabilization, i.e. control of the electric field in the non-conductive Ω_n, is achieved according to the recipe of [3] by incorporating the charge neutrality of Ω_n aside from prescribed charges (i.e. Gauss' law). This extra condition is balanced by an extra unknown that results from the non-direct splitting of the electric scalar potential (φ) into two parts, $\varphi = \tilde{\varphi} + \psi$, with $\psi =$ constant in the conducting domain Ω_c. The final stable formulation in Coulomb gauge is then given by

$$\mathbf{curl}\,\frac{1}{\mu}\,\mathbf{curl}\,\mathbf{A}_k + \left(\frac{\varepsilon}{\triangle t^2} + \frac{\sigma}{\triangle t}\right)\mathbf{A}_k + \left(\frac{\varepsilon}{\triangle t} + \sigma\right)\mathbf{grad}(\tilde{\varphi}_k + \psi_k) \tag{5}$$

$$= \left(\frac{2\varepsilon}{\triangle t^2} + \frac{\sigma}{\triangle t}\right)\mathbf{A}_{k-1} - \frac{\varepsilon \mathbf{A}_{k-2}}{\triangle t^2} + \frac{\varepsilon\,\mathbf{grad}\,(\tilde{\varphi}_{k-1}+\psi_{k-1})}{\triangle t} + \mathbf{j}_k^s + \frac{\mathbf{j}_k^{s\rho}-\mathbf{j}_{k-1}^{s\rho}}{\triangle t} \text{ in } \Omega,$$

$$\mathrm{div}(\varepsilon \mathbf{A}_k) = 0 \text{ in } \Omega, \tag{6}$$

$$\mathrm{div}(\varepsilon\,\mathbf{grad}(\tilde{\varphi}_k + \psi_k)) = \mathrm{div}\mathbf{j}_k^{s\rho} \text{ in } \Omega_n. \tag{7}$$

Note that the additional third equation (7) is independent of the timestep $\triangle t$, which achieves the stabilization. We chose the Coulomb gauge as typical gauge for the low frequency range, but this is not mandatory.

To cast (5) and (7) into weak form, we have to introduce an appropriate function space for the extra unknown ψ_k: $H_n^1 := \{\psi \in H_0^1(\Omega)\colon \psi_{|\Omega_c} \equiv \text{const}\}$. The function spaces for the other unknowns follow from standard choices, see [2, Sect. 5] for notations and details. Then the variational formulation reads: seek $\mathbf{A}_k \in \boldsymbol{H}_0(\mathbf{curl}, \Omega)$, $\tilde{\varphi}_k \in H_0^1(\Omega)$, $\psi_k \in H_n^1(\Omega)$ such that

$$\left\langle \frac{1}{\mu}\,\mathbf{curl}\,\mathbf{A}_k,\, \mathbf{curl}\,\mathbf{A}' \right\rangle + \left\langle \left(\frac{\varepsilon}{\triangle t^2} + \frac{\sigma}{\triangle t}\right)\mathbf{A}_k,\, \mathbf{A}' \right\rangle \tag{8}$$

$$+ \left\langle \left(\frac{\varepsilon}{\triangle t} + \sigma\right)\mathbf{grad}(\tilde{\varphi}_k + \psi_k),\, \mathbf{A}' \right\rangle = \left\langle \left(\frac{2\varepsilon}{\triangle t^2} + \frac{\sigma}{\triangle t}\right)\mathbf{A}_{k-1} - \frac{\varepsilon}{\triangle t^2}\mathbf{A}_{k-2},\, \mathbf{A}' \right\rangle$$

$$+ \left\langle \frac{\varepsilon}{\triangle t}\,\mathbf{grad}(\tilde{\varphi}_{k-1} + \psi_{k-1}),\, \mathbf{A}' \right\rangle + \left\langle \mathbf{j}_k^s,\, \mathbf{A}' \right\rangle + \left\langle \frac{\mathbf{j}_k^{s\rho} - \mathbf{j}_{k-1}^{s\rho}}{\triangle t},\, \mathbf{A}' \right\rangle \text{ in } \Omega,$$

$$\left\langle \varepsilon \mathbf{A}_k\,,\, \mathbf{grad}\,\tilde{\varphi}' \right\rangle = 0 \text{ in } \Omega, \tag{9}$$

$$\left\langle (\varepsilon\,\mathbf{grad}(\tilde{\varphi}_k + \psi_k))\,,\, \mathbf{grad}\,\psi' \right\rangle = \left\langle \mathrm{div}\mathbf{j}_k^{s\rho}\,,\, \psi' \right\rangle \text{ in } \Omega_n. \tag{10}$$

for all $\mathbf{A}' \in \boldsymbol{H}_0(\mathbf{curl}, \Omega)$, $\varphi' \in H_0^1(\Omega)$, and $\psi' \in H_n^1(\Omega)$.

Remark: We point out that the solution cannot be unique, because (10) can be obtained by testing (8) with $\mathbf{A}' := \mathbf{grad}\,\psi'$, $\psi' \in H_n^1(\Omega)$.

4 Numerical Experiments

We employ a conformal Galerkin finite element discretization of (8)–(10) based on first order edge elements for the vector potential and first order nodal elements for the scalar potentials [2, Sect. 3]. This was implemented in an in-house simulation framework at ABB.

According to the above remark, we face a *singular* linear system of equations with consistent right hand side in each timestep. Iterative solvers can tackle this kind of problem and we used a preconditioned BiCGstab method to solve the system. We constructed a preconditioner by using the direct solver Pardiso [7] for solving the regularized system that results from applying a lower conductivity bound of

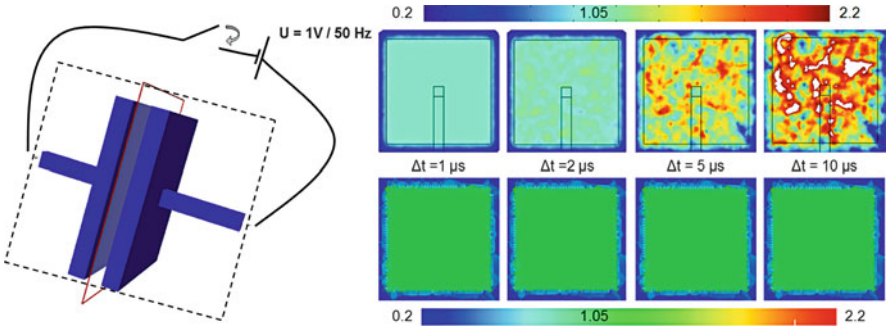

Fig. 1 *Left:* Plate capacitor. *Right:* Electric field in [V/m] after 100 μs in the center between the capacitor plates (solid red plane) for different timesteps. The upper row shows the solutions of the system (3)–(4), and the lower row shows the solutions of the stabilized system (8)–(10). Please note the different color-scales due to the different visualization software. The expected value is 1.05 V/m. A mesh of 200,000 elements was used in both cases

1 $(\Omega \mathrm{m})^{-1}$ in (8). Note that this expensive preconditioner is almost identical to a direct solver, because the regularized system differs only slightly from (8)–(10). An alternative is probably the cheaper preconditioner that was introduced for frequency domain in [6], but that has not yet been transferred to time domain.

In order to compare formulations, we used the RF module of the commerical software COMSOL [1] (with the direct solver Pardiso) for the solution of the standard non-stabilized formulation in temporal gauge (3) and (4). A simple rectangular plate capacitor with plate distance of 3 cm and plate diameter of 43 cm was computed. We switched on a sinusoidal voltage of 1 V/50 Hz. Figure 1 shows the greatly improved robustness of the stabilized system.

For the standard system (3) and (4) one encounters a severe stability constraint on the timestep, despite the use of implicit timestepping, and the electric field is disturbed for timesteps larger than 1 μs. We observed that the disturbance started even earlier, at timesteps of 0.5 μs for a larger mesh with one Million elements. This timestep constraint is much more relaxed for the stabilized system (8)–(10), where we could use three orders of magnitude larger timesteps of 1 ms. This is confirmed by a comparison with a computation in the frequency domain, see Fig. 2.

5 Lightning Impulse Test Simulation

As a practical example we simulated the lightning impulse test of an ABB dry-type transformer.

Power and distribution transformers are not only exposed to the rated voltage over their life time; occasionally, transformers can experience transient voltage surges produced by network switching operations or atmospheric overvoltages. The insulation between the windings has to be very carefully designed to ensure

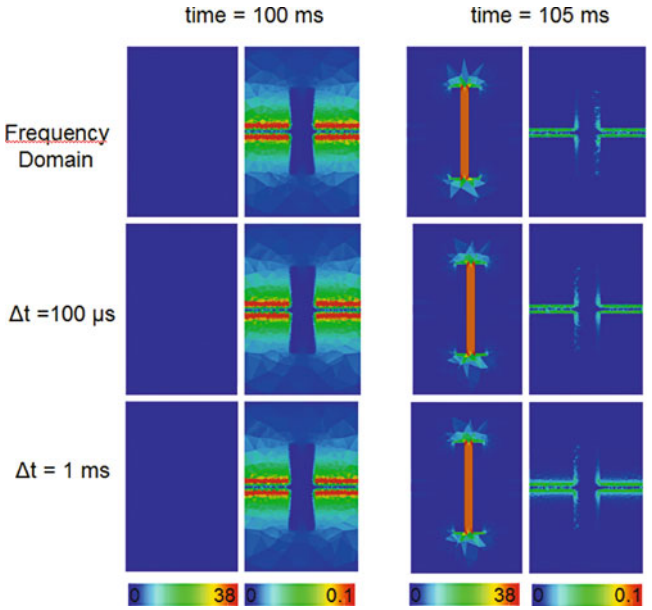

Fig. 2 Comparison of the electric field (0 − 38 V/m) and the magnetic field (0 − 0.1 pT) between the solution in frequency domain, and the solution in time domain for timesteps of 1 ms and 100 μs. The fields are shown after a steady oscillation is reached (i.e. here after five periods of 20 ms) at the zero-voltage-intersect after 100 ms and at the peak voltage after 105 ms. The pictures are in the dashed black plane of the capacitor in Fig. 1

reliable operation even if a voltage surge occurs. This is tested experimentally by the lightning impulse test which is precisely defined by the IEC standard [5]. Due to the lack of insulating oil in dry-type transformers, more sophisticated dielectric design is required compared to the oil-immersed counterparts. Thus the dielectric design of dry-type transformers can be strongly supported by electromagnetic field simulations of the lightning impulse test. An accurate simulation of the electric field between the winding sections is therefore of paramount importance.

The configuration for the lightning impulse test is shown in Fig. 3. The peak value of the applied impulse voltage is roughly five times the nominal voltage. The 1.2 μs rise time and 50 μs decay time of the voltage in the lightning impulse test are specified to mimic the real nature of the surge, see [5]. The Fourier spectrum of the applied signal comprises waves with wavelengths comparable to the size of the windings. The propagation of the waves along the windings can produce local field enhancement regions that are caused by both multiple reflections of the electromagnetic waves and internal resonance effects by the interaction of the capacitances and inductances of the windings. Due to the complex winding geometries, it is practically impossible to predict critical field regions of the windings without performing transient full Maxwell simulations. Taking into account only static simulations may strongly falsify the estimation of a possible dielectric breakdown.

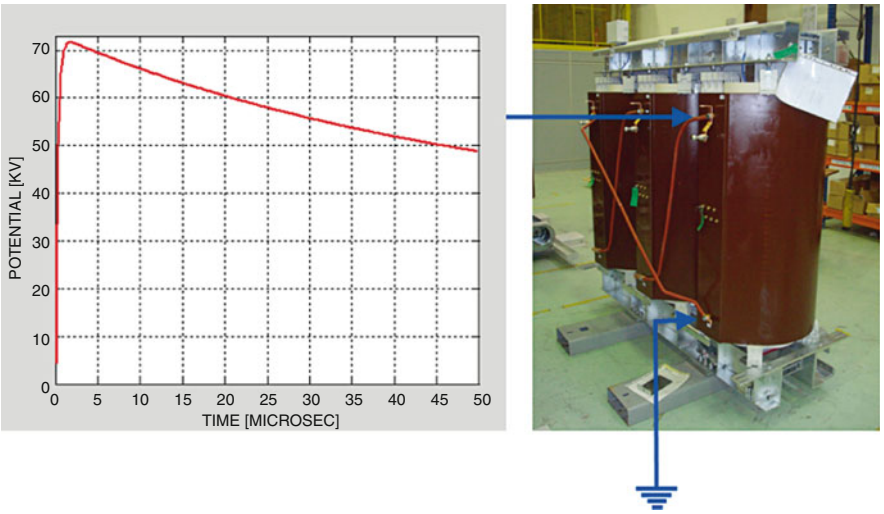

Fig. 3 Dry-Transformer and applied test voltage pulse

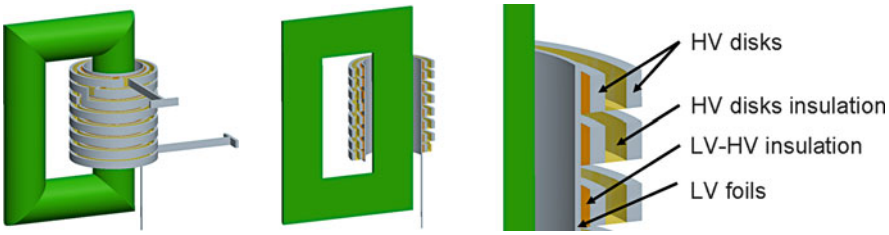

Fig. 4 Transformer model showing windings and core (*left*), its cross-section (*center*), and the details of the winding disks (*right*)

However, the windings in their full complexity cannot be modeled in 3D: Each disk consists of several tens of turns of conductive foil with a thickness in the range of some hundred microns. The foils are insulated against each other. The thickness of the insulation is even smaller than the thickness of the conductive foil. This yields a huge aspect ratio compared to the height of about 2 m of the transformer. Therefore, the internal structure of the winding sections is simplified. Effective values of the dielectric permittivity and magnetic permeability are used to model the internal capacitances and inductances of the real winding sections. The regions of the effective material parameters are shown in Fig. 4. They are placed in the regions where the corresponding capacitances (turn-to-turn capacitance of a single winding disk) and inductances (stray field in the cooling channel) are confined. The effective material parameters are derived from 2D computations. An alternative treatment of the windings could be to use the homogenization technique, see [9].

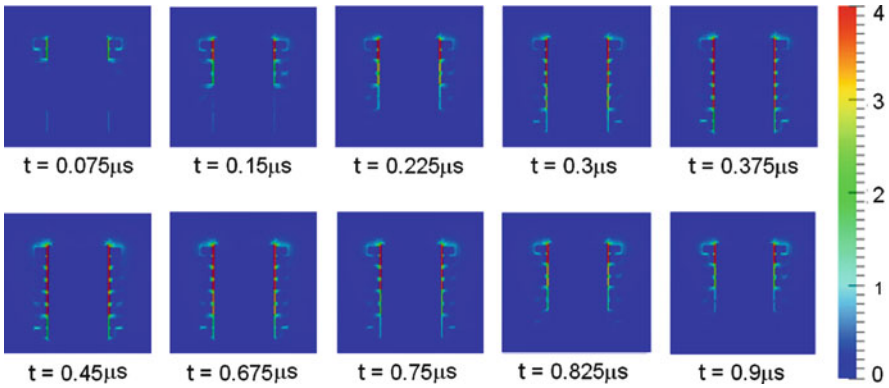

Fig. 5 Electric field distribution (in kV/mm) over the axial symmetry slice (Fig. 4, *center*) shown at different time instants. The propagation and the reflection of the electromagnetic wave is visible. Note that this oscillation is much faster than the applied voltage pulse of Fig. 3

The transient electric field between the windings as computed by an impulse lightning simulation is shown in Fig. 5. One recognizes a reflection during the rise time of 1 μs of the voltage. These reflections continue during the first 10 μs of the simulation. This agrees with the measured oscillations of the electric field between the windings in the experimental lightning impulse test.

6 Conclusion

In this article we introduced a *robust full Maxwell formulation* in time domain. This formulation is stable for large timesteps in simulations of slow processes. We demonstrated the improved stability, compared to standard formulations, by numerical experiments. A three order of magnitude improvement of the timestep was achieved. As an example, we simulated a transient industrial application with coupled capacitive and inductive effects. We conclude that the stabilized formulation (8)–(10) represents a unified Maxwell model that is robust even with large timesteps.

References

1. Comsol website, URL http://www.comsol.com
2. Hiptmair, R.: Finite elements in computational electromagnetism. Acta Numerica **11**, 237–339 (2002)
3. Hiptmair, R., Krämer, F., Ostrowski, J.: A robust Maxwell formulation for all frequencies. IEEE Trans. Magn. **44**(6), 682–685 (2008)

4. Hiptmair, R., Sterz, O.: Current and voltage excitations for the eddy current model. Int. J. Numer. Model **18**(1), 1–21 (2005)
5. International standard IEC 60076-11: Dry-type transformers. International Electrotechnical Commission, Geneve, Switzerland (2004)
6. Ostrowski, J., Bebendorf, M., Hiptmair, R., Krämer, F.: H-matrix based operator preconditioning for full maxwell at low frequencies. IEEE Trans. magn. **46**(8), 3193–3196 (2010)
7. Pardiso website, www.pardiso-project.org
8. van Rienen, U.: Numerical methods in computational electrodynamics. In: Lecture Notes in Computational Science and Engineering, vol. 12. Springer, Berlin (2001)
9. Sabariego, R., Dular, P., Gyselinck, J.: Time-domain homogenization of windings in 3-d finite element models. IEEE Trans. magn. **44**(6), 1302–1305 (2008)
10. Schmidt, K., Sterz, O., Hiptmair, R.: Estimating the eddy-current modelling error. IEEE Trans. Magn. **44**(6), 686–689 (2008)
11. Steinmetz, T., Kurz, S., Clemens, M.: Domains of validity of quasistatic and quasistationary field approximations. Submitted to COMPEL **30**(4), 1237–1247 (2011)